World Journal of Advanced Research and Reviews
eISSN: 2581-9615 CODEN (USA): WJARAI
Cross Ref DOI: 10.30574/wjarr
Journal homepage: https://wjarr.com/

(RESEARCH ARTICLE)

DESIGN, LOCAL FABRICATION AND QUALITATIVE TRIAL OF A LOW-COST SINGLE-SCREW EXTRUDER FOR UNFIRED EARTH BRICKS IN GUINEA

Alpha Issa Diallo [1, 2], Kossoko Babatoundé Audace Didavi [2, *], Mariama Bah [1, 2], Thierno Mamoudou Diallo [1, 2], Abdoul Kadri Diallo [1, 2] and Constant Agnimoan Alihonou [1, 2]

[1] Department of Mechanical Design and Manufacturing, Mamou Higher Institute of Technology (IST Mamou), BP 63, Mamou, Guinea.
[2] IST Mamou Applied Science Research Laboratory, Mamou Higher Institute of Technology, Mamou, Guinea.
* Corresponding Author

ORCID Details
Kossoko Babatoundé Audace Didavi: https://orcid.org/0000-0002-8114-8677
Abdoul Kadri Diallo: https://orcid.org/0000-0001-6429-0180
Constant Agnimoan Alihonou: https://orcid.org/0009-0004-7591-0751

World Journal of Advanced Research and Reviews, 2026, 32(02), 1619–1635

Publication history: Received on 12 October 2026; revised on 16 November 2026; accepted on 18 November 2026

Article DOI: https://doi.org/10.30574/wjarr.2026.32.2.2984

Copyright © 2026 Author(s) retain the copyright of this article. This article is published under the terms of the Creative Commons Attribution License 4.0

ABSTRACT

Earth is the main walling material in Guinea, where more than half of households lived in earth-walled dwellings in 2014, yet the machines that shape earth bricks have received less attention than the material itself. This paper reports the design, local fabrication and first qualitative trial of a semi-automatic single-screw extruder built in the workshop of the Mamou Higher Institute of Technology from standard steel sections with conventional machine tools. The machine is driven by a 1.5 kW gear motor at 82 rpm; a 122 mm screw with a stepped pitch (122/97/61 mm) rotates in a 125 mm barrel and feeds a convergent die that forms a 100 × 100 mm column, wire-cut into 200 mm bricks. The sizing was re-derived with a single consistent set of assumptions. At the 150 kg/h design target the column advances at 2.3 mm/s (about 42 bricks per hour), which is 2.5% of the geometric displacement of the metering zone; throughput therefore does not constrain the geometry. The 30 mm C45 shaft has a yield safety factor of 5.0 at rated torque and 2.0 at a breakdown torque taken as three times rated. A power-screw estimate shows that rated torque can sustain a die-entry pressure of only 0.36–0.58 MPa, below the 1.2 MPa design value, and an annular-plate model shows that the 3 mm flights reach yield at a pressure difference of 0.18 MPa per flight: the flights, not the shaft, govern the admissible pressure, and flights about 7 mm thick would be needed for 1.2 MPa. Finite-element analyses of the screw and chassis, used qualitatively because their load values were not archived, place the maximum screw stress at the root of a flight. In the trial, the prototype extruded a continuous column with minor surface defects. Throughput, power demand and brick properties were not measured; a test protocol is proposed for this purpose. The prototype cost 10.6 million Guinean francs (about USD 1 200).

Keywords: Earth construction, Unfired brick, Auger extrusion, Single-screw extruder, Machine design, Local manufacturing, Appropriate technology.

1 INTRODUCTION

Earth is the most common walling material in Guinea. In the 2014 census, 48.8% of households lived in dwellings whose walls were made of unfired brick or rammed earth (68.4% in rural areas), and a further 5.2% in stabilised earth brick (Fig. 1) [1]. In the Mamou region, where this work was carried out, unfired earth (43.2%) and fired clay brick (44.5%) together account for almost nine households in ten, whereas cement blocks dominate in urban areas (65.3%). Unfired bricks avoid the fuel consumed by kiln firing: the manufacture of unfired clay bricks is reported to release about 80% less CO_2 than that of fired bricks [2], and earth blocks are increasingly considered for low-cost social housing [3, 4].

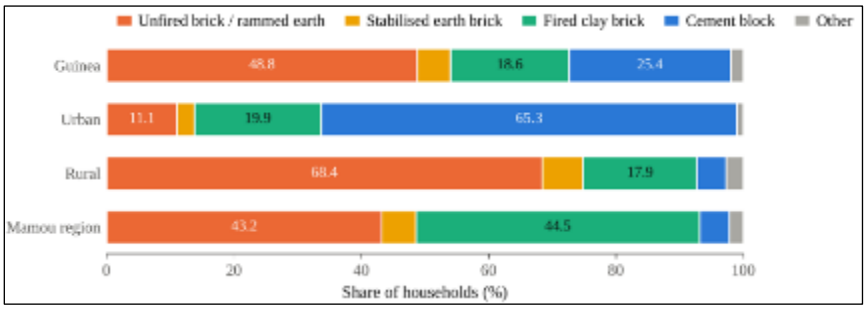


Figure 1: Main wall material of households in Guinea by area of residence and in the Mamou region, from the 2014 General Population and Housing Census. Data from [1]

Most research on earth blocks concerns the material: soil selection, stabilisers, fibres and the resulting mechanical, thermal and durability properties [4]. The production process has received less attention, and the processing of earth still rests largely on empirical knowledge [5]. Three shaping routes are in use (Fig. 2) [6]. In moulding, plastic earth is placed in a mould by hand and the brick is demoulded and sun-dried (adobe). In pressing, a moist but less plastic soil is compacted in a closed mould by a lever, a cam or a hydraulic ram (compressed earth block). In extrusion, plastic earth is pushed continuously through a die by an auger or a piston, and the column is wire-cut into bricks.

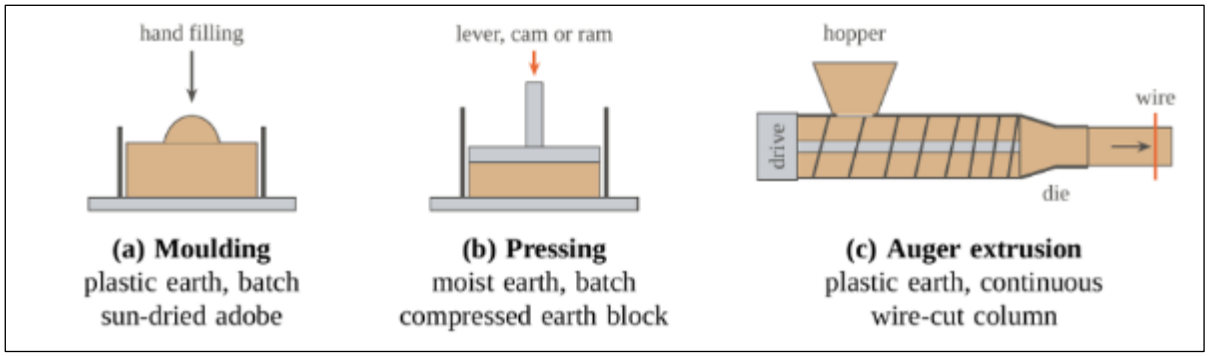


Figure 2: Shaping routes for earth bricks. The machine presented in this paper belongs to route (c)

Machine development for earth blocks has concentrated on presses. Manual presses descend from the CINVA-Ram [6]; recent designs aim at bidirectional compaction with simple kinematics, because the bidirectional manual presses available on the market are mechanically complex, difficult to use and expensive [7]. One such press produced about 30 blocks per hour with three operators [8], and presses of this class are also built by universities to manufacture test blocks [9]. Hydraulic presses reach higher outputs but require pumps, valves and seals that are difficult to source and repair in Guinea.

Auger extrusion is the standard shaping route of the heavy-clay industry; its principles, die design and wear mechanisms are documented for ceramic bodies [10]. Extruded unfired clay bricks are produced industrially in Europe: their compressive strength depends largely on the clay content [11], industrial trials of stabilised unfired bricks have been reported [12], and extruded, wire-cut illitic clay bricks used unfired meet the strength limits of earth-construction standards [2]. Extrusion of earth is also studied for additive manufacturing [13]. At small scale, single-screw extruders have been designed and built from locally available materials for food processing [14], and a prototype clay extruder for small-scale brick making delivered 27 bricks per hour in a performance test [15]. Locally built extruders are rarely documented with a complete and consistent sizing; in particular, whether the drive can generate the assumed extrusion pressure, and whether the screw flights can carry it, is seldom checked.

This paper describes a semi-automatic single-screw extruder for unfired earth bricks, designed and built at the Mamou Higher Institute of Technology (IST Mamou) as a final-year engineering project. A 1.5 kW gear motor drives a stepped-pitch screw that pushes the earth through a convergent die forming a 100 × 100 mm column. The contributions are: (i) a complete and internally consistent sizing of the drive, screw, shaft and die, reproducible with the script provided as supplementary material; (ii) a check of the consistency between the available torque and the assumed extrusion pressure, which identifies the screw flights, not the shaft, as the element that limits the admissible pressure; (iii) a description of a fabrication route using standard steel sections and conventional machine tools, with its cost; (iv) a qualitative account of the first extrusion trial, with the limits of the present evidence and a measurement protocol for the next stage.

The Materials and Methods section describes the design procedure, the data and assumptions, the mathematical model, the finite-element models, the fabrication and the trial. The Results section gives the values computed with the model and their interpretation, the simulations, the trial observations and the cost. The Discussion examines the governing constraints, compares the machine with other small-scale machines, and states recommendations and limitations.

2 MATERIAL AND METHODS

2.1 Methodology

The work followed the seven steps of Fig. 3. The need was translated into a functional specification (step 1), a concept was selected and laid out in CAD (step 2), and the design data and assumptions were fixed (step 3). The drive, screw, shaft, flights and die were then sized with the analytical model described below (step 4). The screw and the chassis were checked by finite-element analysis (step 5), the prototype was fabricated in the institute workshop (step 6), and a first qualitative trial was carried out (step 7). The calculations of the original project were re-derived with a single set of assumptions: the equations of the model are implemented in one script (sizing_check.py, supplementary material), which produces every number reported in the Results.

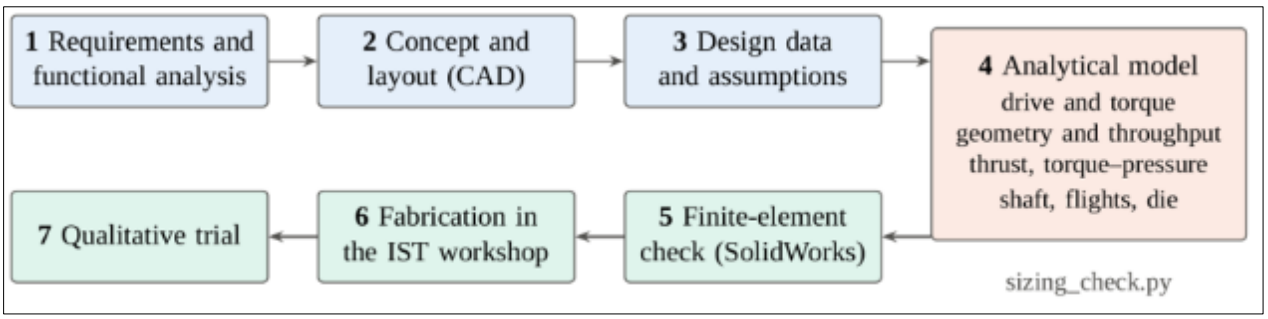


Figure 3: Design and verification procedure. Steps 1–4 define the machine and its analytical model; steps 5–7 check it numerically and experimentally

2.2 Functional analysis and requirements

Table 1: Functional specification (FP: principal function; FC: constraint function)

	Function	Criterion	Level
FP1	Produce unfired earth bricks continuously from moist earth	Throughput	150 [kg/h] (target)
		Brick size	100 × 100 × 200 [mm]
		Shape	solid, rectangular
FC1	Operate on a limited power supply	Installed power	< 3 [kW]
FC2	Be easy to operate	Operation	manual feeding, one start/stop control
FC3	Comply with safety rules	Protection	emergency stop
FC4	Have a low acquisition cost	Manufacture	local materials and workshop
FC5	Be repairable locally	Components	standard sections, bolted drive

The need was analysed with the horned-beast and interactor diagrams, and the service functions were translated into technical solutions with a FAST diagram. Table 1 lists the resulting functional specification. A single-screw extruder was preferred to a press because it produces a continuous column, contains no hydraulic components, and can be made from steel tube, plate and bar available in Guinea. Twin-screw and piston extruders were excluded for their complexity and cost.

2.3 Machine layout

The machine (Fig. 4) consists of a welded IPN chassis (6) carrying a gear motor (1), a hopper (2), a barrel made from steel tube (3) in which the screw rotates, a convergent die (4) and a cutting table (5) on which the column is cut with a steel wire. The screw is driven at one end through a coupling and is free at the die end, so it acts as a cantilever. The shaft runs in rolling bearings at the drive end, where the axial thrust of the screw is reacted by these bearings and by the gear-reducer output; their axial load capacity was not checked.

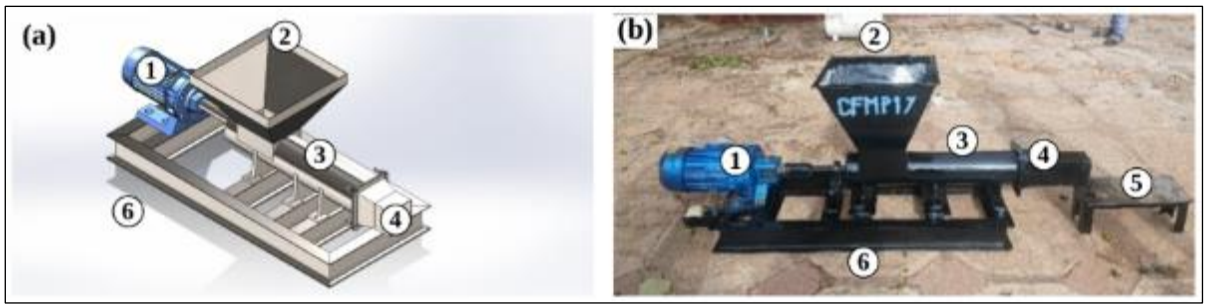


Figure 4: Extruder: (a) CAD model (SolidWorks); (b) fabricated prototype. 1 gear motor; 2 hopper; 3 barrel and screw; 4 die; 5 cutting table; 6 IPN chassis

2.4 Design data and assumptions

Table 2 gathers the data used in the model and states which values were specified, selected or assumed. The flights and the die were made from 3 mm stainless steel sheet whose grade was not recorded; the minimum proof strength of the most common austenitic grade, 1.4301 (cold-rolled), was used [16]. The shaft is made of normalised C45 [17] and the chassis of S235 sections [18]. The assumptions that most affect the results are the extrusion pressure, the friction between earth and steel, and the breakdown torque of the motor; they are examined in the Discussion. Table 3 lists the symbols.

Table 2: Design data and assumptions

Item	Value	Status
Brick (column section $H \times H$, length L_b)	100 × 100 × 200 [mm]	specified
Target throughput Q_m	150 [kg/h]	specified
Wet density of the extruded earth ρ	1800 [kg/m^3]	assumed
Motor	1.5 [kW], 1400 [rpm], 4-pole induction	selected
Gear reducer	coaxial, $i = 17$	selected
Overall drive efficiency η	0.85	assumed
Breakdown-to-rated torque ratio k_b	3.0	assumed (conservative)
Design die-entry pressure p	1.2 [MPa]	assumed
Earth–steel friction angle φ	17–30 [°]	range explored
Screw: outer, root diameter D, d; length L	122, 30; 600 [mm]	selected
Shaft	C45, normalised, $R_e = 305$ [MPa]	selected
Flights and die walls	3 [mm] stainless sheet, 1.4301, $R_{p0.2} = 230$ [MPa]	grade assumed

Elastic constants of steel E, ν	210 [GPa], 0.3	assumed
Barrel	steel tube, bore 125 [mm]	selected
Chassis	IPN 100 sections, S235	selected

Table 3: Main symbols

Symbol	Unit	Meaning	Symbol	Unit	Meaning
A_a	[mm^2]	screw channel annulus area	n_t	[–]	number of turns in a zone
A_d	[mm^2]	die land section, H^2	P, P_1, P_3	[mm]	pitch; feed, metering pitch
A_p	[mm^2]	corner pockets of the die inlet	P_{cr}	[kN]	Euler buckling load
a, b	[mm]	outer, inner radius of a flight	P_h, P_m	[W], [kW]	hydraulic power, motor power
D	[mm]	screw outer diameter	p	[MPa]	die-entry pressure
D_b	[mm]	barrel bore	Δp	[MPa]	pressure difference across one flight
D_p	[N mm]	flexural rigidity of a flight	Q_m, Q_v	[kg/h], [m^3/h]	mass, volumetric throughput
d	[mm]	shaft (root) diameter	Q_g	[m^3/h]	geometric displacement of a zone
E, ν	[MPa], [–]	Young's modulus, Poisson's ratio	q	[N/m]	distributed weight on the shaft
F_a	[N]	axial force on the screw	R_A	[–]	barrel-to-die area ratio
H	[mm]	side of the column	R_e, $R_{p0.2}$	[MPa]	yield, proof strength
h	[mm]	flight height	r_m	[mm]	mean flight radius
i	[–]	gear ratio	S	[–]	safety factor with respect to yield
k	[–]	pitch-to-diameter ratio	T, T_n, T_s	[N m]	torque: general, rated, stall
k_b	[–]	breakdown-to-rated torque ratio	t	[mm]	flight or die-wall thickness
L, L_z	[mm]	screw length, zone length	v	[mm/s]	column velocity
L_c	[mm]	convergent length of the die	w	[mm]	side of a die-wall panel
M, M_r	[N m], [N]	shaft bending moment; radial moment per unit length in a flight	α, α_m	[°]	helix angle at D, at r_m
m_b	[kg]	brick mass	β	[–]	plate stress coefficient
m_s, m_e	[kg]	mass of the screw, of the earth in the barrel	δ	[mm]	deflection of a flight
N	[rpm]	screw speed	η	[–]	overall drive efficiency
n_b	[h^{-1}]	bricks per hour	θ	[°]	half-angle of the die
n_f	[–]	flights carrying the pressure	ρ	[kg/m^3]	wet density of the earth
n_m	[rpm]	motor speed	σ_b , σ_c , σ_{vm}	[MPa]	bending, compressive, von Mises stress
			σ_r, σ_w, τ	[MPa]	flight root, die-wall, shear stress
			φ	[°]	earth–steel friction angle

2.5 Mathematical model

The model links the drive, the screw geometry, the throughput and the loads on the shaft, the flights and the die. Fig. 5 shows the three mechanical sub-models. The equations are written here in symbolic form; their values for the data of Table 2 are given in the Results.

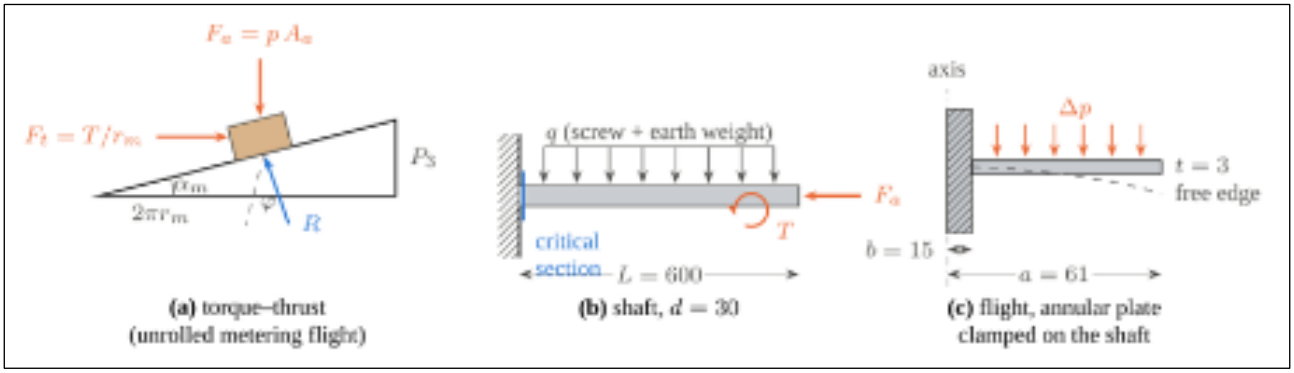


Figure 5: Mechanical models: (a) torque–thrust relation of the metering flight, unrolled as an inclined plane (power-screw analogy); (b) shaft as a cantilever under torsion, axial compression and distributed weight; (c) flight as an annular plate clamped on the shaft and loaded by the pressure difference between its faces (thickness exaggerated, dimensions in mm)

Drive. The screw speed, the rated output torque of the gear motor and the stall torque are

$$N = \frac{n_m}{i}, \qquad T_n = \frac{9550\,P_m\,\eta}{N}, \qquad T_s = k_b\,T_n, \tag{1}$$

with P_m in kW, N in rpm and T in N m. An induction motor can deliver more than its rated torque before stalling: IEC 60034-1 requires polyphase induction motors to withstand an occasional excess torque of 60% [19], and catalogue breakdown torques of small 4-pole motors are typically two to three times the rated value. Since the breakdown torque of the installed motor was not recorded, $k_b = 3$, at the upper end of this range, was used; the stall check of the shaft is therefore conservative.

Barrel and screw geometry. The barrel bore D_b must give a free cross-section larger than the die section $A_d = H^2$, so that the earth is compressed, not expanded, on entering the die:

$$R_A = \frac{\pi(D_b^2 - d^2)}{4A_d} > 1 \quad \Rightarrow \quad D_b > \sqrt{\frac{4A_d}{\pi} + d^2}. \tag{2}$$

The screw has a constant outer diameter D, slightly smaller than D_b, a flight height $h = (D - d)/2$, and three zones of decreasing pitch $P = kD$: feed ($k = 1$), compression ($k = 0.8$) and metering ($k = 0.5$), with lengths of 30, 50 and 20% of the screw length L. For each zone, the number of turns, the helix angle at the outer diameter and the geometric displacement (volume swept per unit time by the channel) are

$$n_t = \frac{L_z}{P}, \qquad \alpha = \arctan\frac{P}{\pi D}, \qquad Q_g = \frac{\pi}{4}\,(D^2 - d^2)\,P\,N. \tag{3}$$

Since the channel depth is constant, the volume per turn is proportional to the pitch, and the volumetric compression ratio of the screw is P_1/P_3.

Throughput. The volumetric flow, the column velocity at the die and the number of bricks per hour at the target throughput Q_m are

$$Q_v = \frac{Q_m}{\rho}, \qquad v = \frac{Q_v}{A_d}, \qquad n_b = \frac{Q_m}{m_b}, \quad m_b = \rho\,H^2 L_b. \tag{4}$$

The flow delivered by an auger extruder is smaller than its displacement Q_g, because the material slips on the barrel wall and the die pressure drives a back flow [10, 20, 21]. These effects were not modelled; the ratio Q_v/Q_g of the metering zone was used only to establish whether the throughput target constrains the geometry.

Axial thrust and torque–pressure consistency. The axial force on the screw was evaluated with the design die-entry pressure acting on the screw channel annulus:

$$F_a = p\,A_a, \qquad A_a = \frac{\pi}{4}\,(D^2 - d^2). \tag{5}$$

To check whether the drive can generate this thrust, the screw was treated as a power screw driving a non-rotating nut, the earth (Fig. 5a), with a friction angle φ between earth and steel. At the mean flight radius $r_m = (D + d)/4$ of the metering zone, the helix angle is $\alpha_m = \arctan[P_3/(2\pi r_m)]$. The maximum pressure that a torque T can sustain, and conversely the torque required for a pressure p, are

$$p_{\max}(T) = \frac{T}{A_a\, r_m \tan(\alpha_m + \varphi)}, \qquad T_{\mathrm{req}}(p) = p\,A_a\, r_m \tan(\alpha_m + \varphi). \tag{6}$$

Eq. 6 neglects the torque spent on shearing the earth and on friction against the barrel, so it overestimates the pressure that the drive can sustain. The friction angle of moist earth on steel was not measured; the range 17–30° was explored. The useful hydraulic power $P_h = p\,Q_v$ was compared with the shaft power.

Shaft. The critical section is at the drive end, where torsion, axial compression and bending act together (Fig. 5b). The shaft was treated as a cantilever of length L carrying the weight of the screw (m_s, shaft and flights) and of the earth filling the barrel (m_e) as a uniform load, which gives an upper bound of the bending moment, since the barrel supports part of the earth:

$$q = \frac{(m_s + m_e)\,g}{L}, \qquad M = \frac{qL^2}{2}. \tag{7}$$

The equivalent stress and the safety factor are [22]

$$\sigma_{vm} = \sqrt{(\sigma_c + \sigma_b)^2 + 3\tau^2}, \quad \sigma_c = \frac{4F_a}{\pi d^2}, \quad \sigma_b = \frac{32M}{\pi d^3}, \quad \tau = \frac{16T}{\pi d^3}, \quad S = \frac{R_e}{\sigma_{vm}}, \tag{8}$$

evaluated at $T = T_n$ and $T = T_s$. Two further checks were made: the minimum diameter in torsion at stall according to the Tresca criterion, and Euler buckling of the shaft as a fixed–free column under F_a, ignoring the stiffening effect of the flights:

$$d_{\min} = \left(\frac{32\,S\,T_s}{\pi R_e}\right)^{1/3}, \qquad P_{cr} = \frac{\pi^2 EI}{4L^2}, \quad I = \frac{\pi d^4}{64}. \tag{9}$$

Flights. Each flight was modelled as a flat annular plate of thickness t, clamped on the shaft ($r = b = d/2$) and free at the outer radius ($r = a = D/2$), loaded by the pressure difference Δp between its two faces (Fig. 5c). The deflection $\delta(r)$ obeys the axisymmetric Kirchhoff plate equation, whose general solution is [23]

$$\frac{1}{r}\frac{d}{dr}\left\{r\,\frac{d}{dr}\left[\frac{1}{r}\frac{d}{dr}\left(r\,\frac{d\delta}{dr}\right)\right]\right\} = \frac{\Delta p}{D_p}, \qquad \delta(r) = C_1 + C_2 r^2 + C_3 \ln r + C_4 r^2 \ln r + \frac{\Delta p\, r^4}{64\, D_p}, \tag{10}$$

with the flexural rigidity $D_p = Et^3/[12(1 - \nu^2)]$. The constants C_1 to C_4 follow from the boundary conditions $\delta(b) = \delta'(b) = 0$ at the clamped edge and $M_r(a) = 0$, $Q_r(a) = 0$ at the free edge, where $M_r = -D_p(\delta'' + \nu\,\delta'/r)$ is the radial bending moment and Q_r the shear force per unit length. The largest stress is the radial bending stress at the root, $\sigma_r = 6\,M_r(b)/t^2$. It is proportional to Δp and, since M_r does not depend on D_p, inversely proportional to t^2. Hence the root yields at $\Delta p_y = R_{p0.2}/(\sigma_r/\Delta p)$; if n_f flights share the pressure build-up equally, the die-entry pressure at yield is $p_y = n_f\,\Delta p_y$, and the thickness needed to carry a pressure p with a safety factor S is

$$t_{\mathrm{req}} = t_0 \sqrt{\frac{S\,p}{n_f\,\Delta p_{y,0}}}, \tag{11}$$

where $\Delta p_{y,0}$ is the yield pressure difference of a flight of thickness t_0. The model neglects the helix angle and the fact that a single turn is not a closed ring; both make the real flight more flexible, so the model is not conservative.

Die. The die converges from a square inlet whose side equals the barrel bore D_b to the $H \times H$ land, a reduction $\Delta h = (D_b - H)/2$ per side. A half-angle θ of at most 15° was used as a design rule for plastic bodies, which sets the minimum convergent length. Because the bore is circular and the inlet square, the four corners of the inlet form pockets of area A_p that the screw does not sweep directly. The die walls were checked as square plates of side $w = H$ clamped on all edges [23], which gives the wall stress and the thickness required for a safety factor S:

$$L_c = \frac{\Delta h}{\tan\theta}, \qquad A_p = D_b^2\left(1 - \frac{\pi}{4}\right), \qquad \sigma_w = \beta\,\frac{p\,w^2}{t^2}, \qquad t_{\mathrm{req}} = w\sqrt{\frac{\beta\,p\,S}{R_{p0.2}}}, \tag{12}$$

with $\beta = 0.3078$ for a clamped square plate with $\nu = 0.3$.

2.6 Finite-element models

Linear static analyses of the screw and of the chassis were carried out in SolidWorks Simulation (Table 4). The output plots of the chassis (axial and bending stress) indicate a beam model of the welded sections. The mesh parameters and the load values were not archived with the models. The finite-element results are therefore used qualitatively (location of the maximum stress, deformed shapes), and the strength assessment relies on the analytical model.

Table 4: Finite-element model settings

	Screw	**Chassis**
Model	solid (shaft and flights)	beam elements (welded sections)
Material (library)	AISI 1045 cold-drawn, $R_e = 530$ [MPa]	ASTM A36, $R_e = 250$ [MPa]
Mesh	tetrahedral solid elements; size not archived	beam elements; number not archived
Fixtures	fixed at the drive-end coupling	support points (zero displacement)
Loads	service loads of the screw; values not archived	weights of the supported parts; values not archived

2.7 Fabrication

All parts were made in the IST Mamou workshop with conventional tools (Fig. 6). The dimensions of the 2D drawings were marked on the raw steel with a square, a rule and a scriber (a). IPN sections, angles and plates were cut with an angle grinder (b) and drilled (c). The shaft and the coupling were turned on a centre lathe (d). The flights were cut from 3 mm sheet, formed and welded on the shaft at the three pitches. The chassis, the barrel and the hopper were assembled by manual metal-arc welding (e, f). The gear motor, the bearings and the screw were bolted, so that they can be removed for maintenance. The machine was then painted (Fig. 4b).

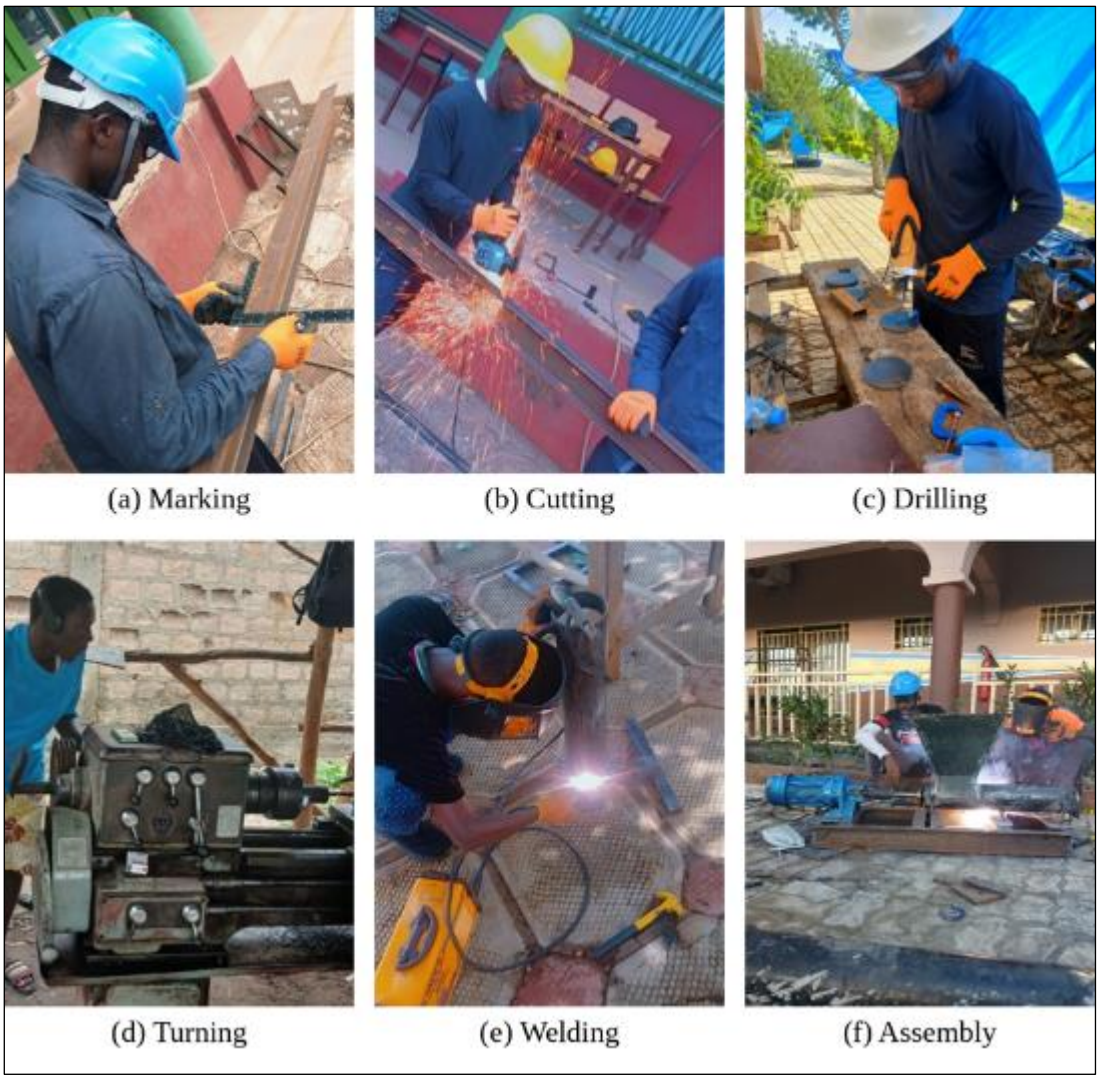


Figure 6: Fabrication steps in the IST Mamou workshop

2.8 Trial

The prototype was first run empty, then loaded with moist earth fed by hand into the hopper. The earth was a local clay soil, mixed manually with water; no stabiliser was reported. The column was cut into bricks with a steel wire on the cutting table. Observations were visual; no quantity was measured.

3 RESULTS

3.1 Drive

With $n_m = 1400$ rpm and $i = 17$, Eq. 1 gives a screw speed $N = 82.4$ rpm and a rated torque at the screw $T_n = 148$ N m. The IEC minimum excess torque is 237 N m and the assumed stall torque $T_s = 444$ N m. The shaft power at rated load is $P_m\,\eta = 1.28$ kW. These torques bound the loads used in the following checks.

3.2 Screw geometry and throughput

With $d = 30$ mm and $A_d = 10\,000$ mm^2, Eq. 2 requires a bore larger than 116.8 mm. A tube with a 125 mm bore was used, which gives $R_A = 1.16$; the screw outer diameter is $D = 122$ mm (radial clearance 1.5 mm) and the flight height $h = 46$ mm. Table 5 gives the geometry of the three zones obtained with Eq. 3, and Fig. 7 shows the screw as built. The as-built pitches are 122, 97 and 61 mm, so the volumetric compression ratio is 2.0; the screw has 6.5 turns in total, and the geometric displacement decreases from 6.62 m^3/h in the feed zone to 3.31 m^3/h in the metering zone.

Table 5: Screw geometry ($D = 122$ mm, $d = 30$ mm, $N = 82.4$ rpm)

	Feed	Compression	Metering
Pitch ratio $k = P/D$ [–]	1.0	0.8	0.5
Pitch P [mm]	122	97	61
Zone length L_z [mm]	180	300	120
Number of turns n_t [–]	1.48	3.09	1.97
Helix angle at D, α [°]	17.7	14.2	9.0
Geometric displacement Q_g [m^3/h]	6.62	5.26	3.31

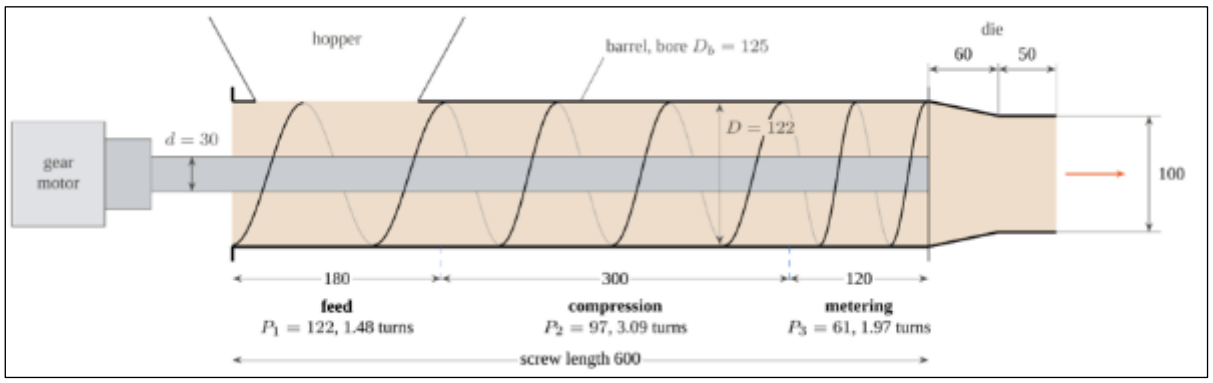


Figure 7: Screw, barrel and die drawn to scale (dimensions in mm). The flight edges are the projections of the helix at the outer diameter; the rear half of each turn is shown in grey

At the 150 kg/h target, Eq. 4 gives $Q_v = 0.0833$ m^3/h and a column velocity of 2.3 mm/s. The target is therefore 2.5% of the geometric displacement of the metering zone. A brick of 3.6 kg leaves the die every 86 s, i.e. 42 bricks per hour or about 330 bricks in an 8-hour shift. Two conclusions follow. First, the throughput target does not constrain the geometry, which is set by the die section and the area ratio of Eq. 2. Second, the output of the machine is governed by wall slip and back flow, which were not modelled; the delivered throughput can only be obtained by measurement (Appendix).

3.3 Axial thrust and torque–pressure consistency

The channel annulus is $A_a = 10\,983$ mm^2, so the design pressure of 1.2 MPa produces an axial force $F_a = 13.2$ kN (Eq. 5). In the metering zone, $r_m = 38$ mm and $\alpha_m = 14.3°$. Fig. 8a plots Eq. 6. At rated torque, the maximum die-entry pressure is 0.58 MPa for $\varphi = 17°$ and 0.36 MPa for $\varphi = 30°$. Reaching 1.2 MPa would require 305 to 489 N m at the screw, i.e. 2.1 to 3.3 times the rated torque. Within the explored friction range, the design pressure is therefore reached only near the breakdown torque of the motor, and the steady-state pressure in operation is expected to be well below 1.2 MPa. The hydraulic power $p\,Q_v$ at the design point is 28 W, about 2% of the rated shaft power: almost all the power is dissipated by friction and shearing of the earth.

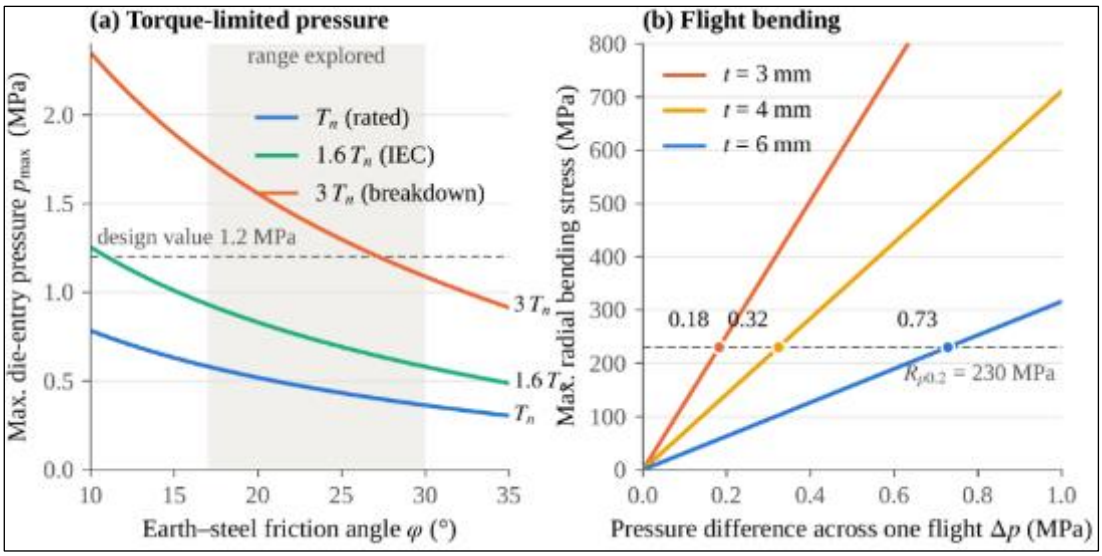


Figure 8: (a) Maximum die-entry pressure that the drive can sustain (Eq. 6) as a function of the earth–steel friction angle, for the rated torque T_n, the IEC minimum excess torque $1.6\,T_n$ and the assumed breakdown torque $3\,T_n$. (b) Maximum radial bending stress in one flight modelled as an annular plate clamped on the shaft (Eq. 10), for three flight thicknesses; the dots mark the pressure difference at which the root yields

3.4 Shaft

The screw weighs 5.0 kg (shaft 3.3 kg, flights 1.7 kg) and the earth filling the barrel 12.1 kg, so Eq. 7 gives $q = 280$ N/m and an upper-bound bending moment $M = 50.4$ N m at the drive end. Table 6 lists the results of Eqs. 8 and 9. The 30 mm shaft has a yield safety factor of 5.0 at rated torque and 2.0 at the assumed breakdown torque. Torsion dominates the equivalent stress at stall, while the compressive and bending stresses (18.6 and 19.0 MPa) are small. The Tresca diameter at stall with $S = 1.5$ is 28.1 mm, below the 30 mm used, and the Euler load of the shaft alone is 4.3 times the design thrust. The shaft is therefore not the critical element of the screw.

Table 6: Analytical strength checks

Element	Quantity	Value
Shaft, $d = 30$ [mm]	Compressive stress σ_c (13.2 [kN]) [MPa]	18.6
	Bending stress σ_b (cantilever, 50.4 [N m]) [MPa]	19.0
	Shear stress τ at T_n / at $3T_n$ [MPa]	27.9 / 83.7
	Von Mises stress at T_n / at $3T_n$ [MPa]	61.3 / 149.7
	Safety factor $S = R_e/\sigma_{vm}$ at T_n / at $3T_n$ [–]	5.0 / 2.0
	Tresca minimum diameter at $3T_n$, $S = 1.5$ [mm]	28.1
	Euler load (fixed–free) [kN] / ratio to F_a [–]	57.2 / 4.3
Flight, $t = 3$ [mm]	Root stress per unit Δp [MPa/MPa]	1264
	Δp at yield ($R_{p0.2} = 230$ [MPa]) [MPa]	0.18
	Die-entry pressure at yield, $n_f = 2$ [MPa]	0.36
Die wall, $t = 3$ [mm]	Stress per unit pressure ($w = 100$ [mm]) [MPa/MPa]	342
	Thickness for $\sigma_w \leq R_{p0.2}/1.5$ at 1.2 [MPa] [mm]	4.9

3.5 Flights

The flights are the critical element (Fig. 8b). For $t = 3$ mm, the solution of Eq. 10 gives a root stress of 1264 MPa per MPa of pressure difference, so the root yields at $\Delta p = 0.18$ MPa. If the pressure is built up over the two turns of the metering zone ($n_f = 2$), the flights yield when the die-entry pressure reaches about 0.36 MPa, at the lower end of the

range that the drive sustains at rated torque. Flights 6 mm thick would yield at $\Delta p = 0.73$ MPa, i.e. at a die-entry pressure of about 1.5 MPa over two turns, 1.21 times the design value. With Eq. 11, carrying 1.2 MPa with $S = 1.5$ requires flights 6.7 mm thick if the pressure builds up over two turns and 5.4 mm thick over three.

3.6 Die

With $\Delta h = 12.5$ mm, the 15° rule of Eq. 12 requires a convergent length of at least 46.7 mm; 60 mm was adopted, which gives a half-angle of 11.8° (Fig. 9b). The land length is 50 mm, as recorded in the project report. The corner pockets of the 125 mm inlet (Fig. 9a) total 3353 mm^2, or 21% of the inlet section; in these pockets the earth is not pushed directly by the screw and may stagnate. Conversely, the corners of the 100 × 100 mm land lie outside the bore circle, so the earth must flow outwards to fill them. The 3 mm die walls reach 342 MPa per MPa of pressure: 410 MPa at the design pressure, above the proof strength, and 125 to 200 MPa at the torque-limited pressures. A wall thickness of 4.9 mm, or external stiffeners, would keep the walls below $R_{p0.2}/1.5$ at 1.2 MPa.

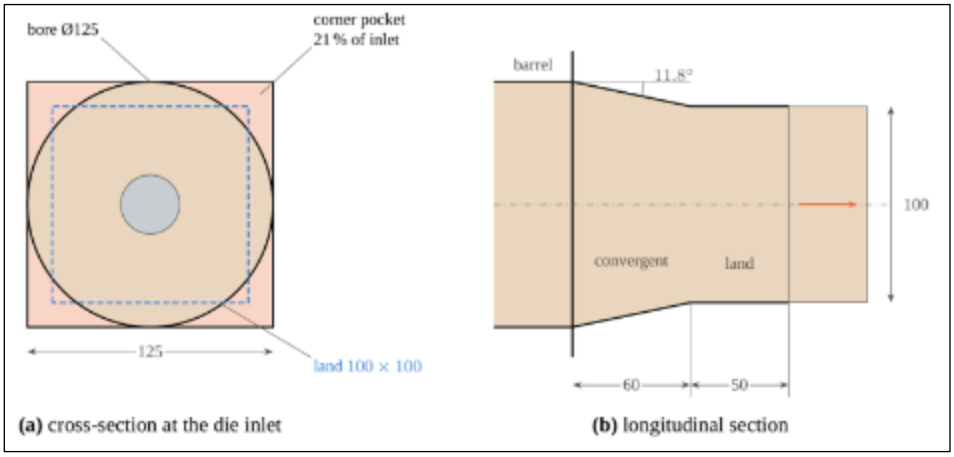


Figure 9: Die geometry (mm). (a) Circular barrel bore inside the square die inlet; corner pockets shaded, land section dashed. (b) Convergent section and land

3.7 Finite-element results

Fig. 10 shows the stress and displacement fields, and Table 7 summarises the results; since the load values were not archived, the magnitudes are given for information. In the screw, the maximum von Mises stress, 149.7 MPa, is located at the root of the first flight next to the fixed end. With the library yield strength of 530 MPa, the minimum safety factor is 3.5; with the yield strength of normalised C45 (305 MPa), it would be 2.0. The maximum displacement, 0.52 mm, occurs at the free end and is smaller than the 1.5 mm radial clearance. In the chassis, the maximum combined axial and bending stress of 167 MPa occurs in the longitudinal members, the maximum deflection of 2.0 mm at their mid-span, and the minimum safety factor is 1.5 with respect to 250 MPa (1.4 with respect to the 235 MPa of S235).

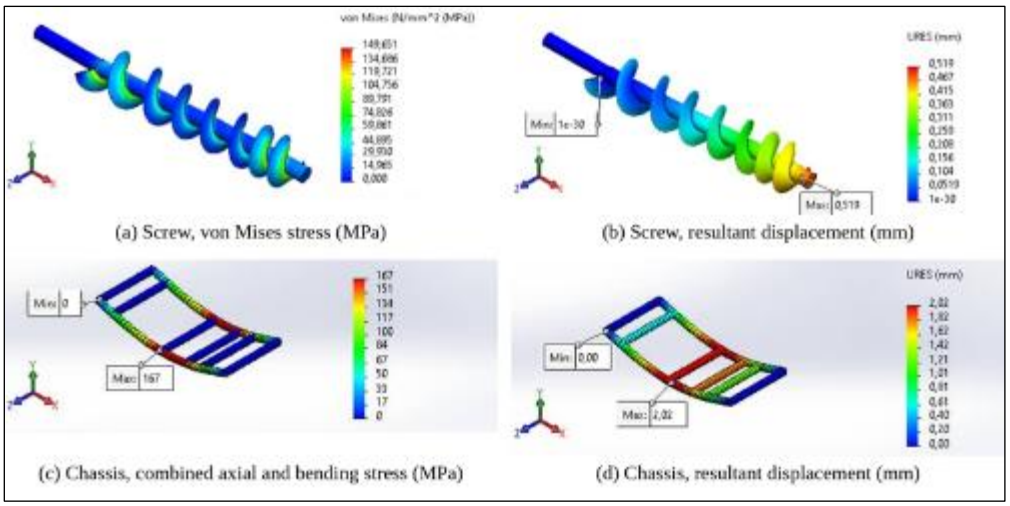


Figure 10: Finite-element results (SolidWorks Simulation; deformed shapes exaggerated)

Table 7: Finite-element results

Part	Max. stress	Location	R_e used	Min. safety	Max. displacement
	[MPa]		[MPa]	factor [–]	[mm]
Screw	149.7	root of first flight	530	3.5	0.52 (free end)
Chassis	167	longitudinal members	250	1.5	2.0 (mid-span)

3.8 Fabrication and operation

The prototype was completed in the IST Mamou workshop with the tools described above. Two operations required the most effort. First, the helical flights were formed and welded by hand, without the dedicated machines normally used to form helical sections. Second, the screw axis had to be aligned with the gear-reducer output and the shaft bearings to avoid vibration and wear. Operating rules were drawn up for the prototype: the coupling, the bolts and the emergency stop are checked before each start; the hopper and barrel are inspected for stones; the bearings are greased every 72 h; the barrel is emptied and cleaned after each use, because earth that dries inside can block the screw at the next start; and the thickness of the flights is monitored for abrasive wear.

3.9 Trial observations

After the final alignment, the no-load run was smooth and without rubbing. Under load, the machine extruded a continuous 100 × 100 mm column that was cut into bricks with a wire (Fig. 11). The bricks kept their shape after cutting and handling. Two defects were observed: longitudinal grooves and irregularities on the faces, visible in Fig. 11b, and edges that crumbled locally. They are attributed to the variation of the moisture content of the manually mixed earth and to the as-welded inner surface of the die, which increases wall friction; neither attribution was tested.

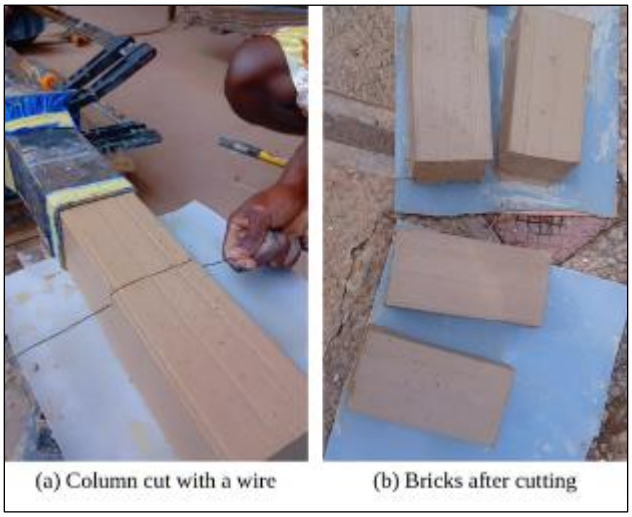


Figure 11: First extrusion trial

3.10 Cost

Table 8 gives the cost of the prototype. The materials and bought-in components (gear motor, steel sections, tube, sheet, bearings and consumables) account for 94% of the total. The project report gives only these aggregated amounts.

Table 8: Cost of the prototype (2026; 1 USD ≈ 8800 GNF)

Item	[GNF]	[USD]
Materials and bought-in components	10 000 000	1136
Labour	600 000	68
Total cost	10 600 000	1205
Selling price with 25% margin	13 250 000	1506

4 DISCUSSION

4.1 Governing design constraints

The design target of 150 kg/h does not constrain the geometry: the screw displaces about 40 times this volume in its metering zone, and the flow actually delivered depends on wall slip and die back-pressure [10, 21]. The geometry is set instead by the die section and the barrel-to-die area ratio (Eq. 2), and the admissible pressure by two elements: the available torque and the flights. The shaft is not critical, with a safety factor of 2.0 even at the assumed breakdown torque.

The two limits are of the same order. At rated torque the drive sustains 0.36 to 0.58 MPa at the die entry, while the 3 mm flights yield at about 0.36 MPa if the pressure builds up over two turns (Fig. 12). The flights may therefore be loaded close to yield in normal operation. No permanent deformation of the flights was reported after the trial, which suggests that the pressure reached was lower, but this was not measured. Since the yield pressure of a flight grows with the square of its thickness, a moderate increase in thickness is enough: 6.7 mm for 1.2 MPa with a safety factor of 1.5 if the pressure builds up over two turns, and 5.4 mm over three (Eq. 11). The drive would then need a rated torque of 300 to 490 N m at the screw, two to three times the present value.

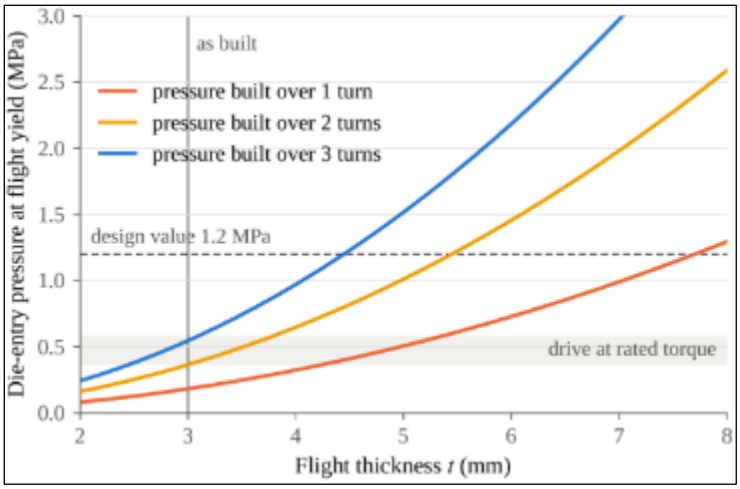


Figure 12: Die-entry pressure at which the flights yield, as a function of flight thickness, when the pressure is built up over one, two or three turns (annular-plate model, $R_{p0.2} = 230$ MPa). The shaded band is the pressure that the drive sustains at rated torque for $\varphi = 17–30°$

4.2 Analytical and numerical results

The load values of the finite-element models were not archived, so the simulated stresses cannot be compared directly with Table 6. Two observations are nevertheless consistent with the analytical results: the maximum stress in the screw model is located at the root of a flight, which the plate model identifies as the critical element, and the maximum displacement of the screw (0.52 mm) is smaller than the radial clearance (1.5 mm), so the flights should not touch the barrel under the simulated loads. The chassis safety factor of 1.5 is acceptable for static loads, but leaves little margin for the vibration and shocks of a workshop machine; a fatigue check of the welded joints would be needed for continuous production.

4.3 Die and surface quality

The corner pockets at the die inlet (Fig. 9a) and the as-welded die surface are plausible causes of the surface defects observed, together with the moisture variation of the manually mixed earth. In clay extrusion, die design aims at a uniform velocity across the column, because velocity differences between the core and the edges cause surface tearing [10]. A die inlet machined to the bore diameter with a gradual round-to-square transition, a ground or lined die surface, and a lubricated land are the corresponding remedies. Mechanical mixing of the earth to a controlled moisture content would remove the other suspected cause.

4.4 Comparison with other small-scale machines

Table 9 places the extruder among small-scale machines for which an output is reported. Its nominal output is of the same order as that of a manual press and of a small clay extruder, but it was not measured, and the unit sizes differ between machines. The extruder needs electricity, which the manual press does not; the number of operators needed

for feeding and cutting was not recorded during the trial. A comparison on a common basis (bricks per hour per operator, energy per brick, brick density and strength) requires the measurements listed in the Appendix.

Table 9: Small-scale machines for earth or clay bricks with a reported output

Machine	Route	Energy	Output [units/h]	Operators	Status
Float-Ram press [8]	pressing	manual	about 30	3	measured
Clay extruder [15]	extrusion	n/a	27	n/a	measured
This work	auger extrusion	electric, 1.5 [kW]	42	not recorded	nominal (not measured)

4.5 Recommendations for a second prototype

The analysis leads to the following changes, in order of priority: (1) flights 7 mm thick (at least 6.7 mm for a safety factor of 1.5 at 1.2 MPa built over two turns), or thinner flights reinforced with gussets at the root (Fig. 12); (2) die walls 5 mm thick or stiffened externally, with an inlet machined to the bore diameter and a ground land; (3) a gear motor whose rated output torque matches the target pressure, and a thrust bearing sized for the axial force at the drive end; (4) a guard on the hopper opening, so that the screw cannot be reached during operation; (5) a current sensor on the motor supply, so that torque and specific energy can be monitored in production.

4.6 Limitations

The evidence presented here has the following limits: (i) throughput, power demand, column velocity and moisture content of the earth were not measured; (ii) the earth was not characterised (particle size distribution, Atterberg limits); (iii) the density, drying shrinkage and compressive strength of the bricks were not measured, so their suitability for masonry is not established; (iv) the extrusion pressure of 1.2 MPa and the friction angle are assumptions; (v) the mesh and load values of the finite-element models were not archived; (vi) fatigue of the rotating shaft and of the welds, and the abrasive wear of the flights, were not assessed; (vii) the machine depends on mains electricity or a generator.

5 CONCLUSION

A semi-automatic single-screw extruder for unfired earth bricks was designed and built with standard steel sections and conventional machine tools in a Guinean technical institute, for about 10.6 million GNF. A consistent re-derivation of the sizing shows that:

- the 150 kg/h target (42 bricks of 100 × 100 × 200 mm per hour) is 2.5% of the geometric displacement of the metering zone and does not constrain the geometry, which is set by the die section and a barrel-to-die area ratio of 1.16;
- the 30 mm C45 shaft has yield safety factors of 5.0 at rated torque and 2.0 at three times rated torque;
- the rated torque of the 1.5 kW drive sustains a die-entry pressure of 0.36 to 0.58 MPa, so the 1.2 MPa design pressure is reached only near the breakdown torque;
- the 3 mm flights yield at a pressure difference of 0.18 MPa per flight and are the critical element; for 1.2 MPa, flights about 7 mm thick and 5 mm die walls are recommended;
- the square die inlet leaves corner pockets covering 21% of its section, a plausible cause, with the as-welded die surface and the manual mixing, of the surface defects observed.

In its first trial, the prototype extruded a continuous column that was wire-cut into bricks. The next step is the measurement campaign described in the Appendix, which will provide the throughput, specific energy and brick properties needed to compare the machine with presses and to validate the design assumptions.

STATEMENTS ON COMPLIANCE WITH ETHICAL STANDARDS

Acknowledgments

The authors thank the students of Group IV (promotion 17, Department of Mechanical Design and Manufacturing), M.M. Diallo, K. Diallo, A.K. Diallo, M. Keita and B. Toupou, who designed and built the prototype in their final-year project, and the workshop staff of IST Mamou.

Disclosure of conflict of interest

The authors declare no conflict of interest.

Data and code availability

The sizing script (sizing_check.py), which produces all the numbers of this paper, and the scripts that draw the figures are provided as supplementary material.

Author contributions

A.I.D.: resources, supervision, project administration. K.B.A.D.: methodology, software, formal analysis, visualisation, writing – original draft. M.B.: conceptualisation, supervision of the fabrication and of the trial. T.M.D. and A.K.D.: investigation, writing – review and editing. C.A.A.: formal analysis, writing – review and editing. All authors read and approved the final manuscript.

REFERENCES

[1] Institut National de la Statistique: Troisième Recensement Général de la Population et de l'Habitation (RGPH3): caractéristiques des habitations et cadre de vie des populations [Third General Population and Housing Census: housing characteristics and living conditions] (INS, Conakry 2017). Information on https://stat-guinee.org

[2] D. Muheise-Araalia and S. Pavia: Constr. Build. Mater. Vol. 268 (2021), 121118

[3] J. Bredenoord and Y. Kulshreshtha: Sustainability Vol. 15 (2023), 5295

[4] M. Valenzuela, G. Ciudad, J.P. Cárdenas, C. Medina, A. Salas et al.: Renew. Sustain. Energy Rev. Vol. 194 (2024), 114323

[5] E. Keita and A. Perrot: RILEM Tech. Lett. Vol. 8 (2023), p. 141

[6] H. Houben and H. Guillaud: Earth Construction: A Comprehensive Guide (Intermediate Technology Publications, London 1994).

[7] C. Ferraresi, W. Franco and G. Quaglia, in: Proceedings of the ASME 2017 International Mechanical Engineering Congress and Exposition, Vol. 11, ASME, New York (2017), V011T15A025.

[8] M. Sassu, A. Romanazzi, L. Giresini, W. Franco, C. Ferraresi et al.: Eng. Solid Mech. Vol. 6 (2018), p. 89

[9] J.A. Cottrell, M. Ali, A. Tatari and D.B. Martinson: Constr. Build. Mater. Vol. 273 (2021), 121997

[10] F. Händle (Ed.): Extrusion in Ceramics (Springer, Berlin 2007).

[11] A. Heath, P. Walker, C. Fourie and M. Lawrence: Proc. Inst. Civ. Eng. Constr. Mater. Vol. 162 (2009), p. 105

[12] J.E. Oti, J.M. Kinuthia and J. Bai: Proc. Inst. Civ. Eng. Eng. Sustain. Vol. 162 (2009), p. 229

[13] A. Perrot, D. Rangeard and E. Courteille: Constr. Build. Mater. Vol. 172 (2018), p. 670

[14] F.T. Fayose, A.S. Ogunlowo and L.A.S. Agbetoye: J. Eng. Sci. Technol. Vol. 12 (2017), p. 2585

[15] A.V. Angeles: Design, Construction and Performance Test of a Clay Extruder Machine for Small-Scale Brick Making (Graduate thesis, University of the Philippines Los Baños 1987).

[16] EN 10088-2: Stainless Steels – Part 2: Technical Delivery Conditions for Sheet/Plate and Strip of Corrosion Resisting Steels for General Purposes (CEN, Brussels 2014).

[17] EN 10083-2: Steels for Quenching and Tempering – Part 2: Technical Delivery Conditions for Non Alloy Steels (CEN, Brussels 2006).

[18] EN 10025-2: Hot Rolled Products of Structural Steels – Part 2: Technical Delivery Conditions for Non-Alloy Structural Steels (CEN, Brussels 2019).

[19] IEC 60034-1: Rotating Electrical Machines – Part 1: Rating and Performance (International Electrotechnical Commission, Geneva).

[20] Z. Tadmor and C.G. Gogos: Principles of Polymer Processing, 2nd ed. (Wiley, Hoboken 2006).

[21] C. Rauwendaal: Polymer Extrusion, 5th ed. (Hanser, Munich 2014).

[22] R.G. Budynas and J.K. Nisbett: Shigley's Mechanical Engineering Design, 10th ed. (McGraw-Hill, New York 2015).

[23] W.C. Young and R.G. Budynas: Roark's Formulas for Stress and Strain, 7th ed. (McGraw-Hill, New York 2002).

6 APPENDIX: PROPOSED MEASUREMENT PROTOCOL

Table lists the measurements needed to validate the design assumptions and to compare the machine with presses.

Table 10: Measurements planned for the next stage

Quantity	Instrument	Procedure
Throughput	Stopwatch, balance	Mass extruded in 5 min, at least three runs; column velocity over a marked length
Power demand	Clamp ammeter, voltmeter	Current at no load and under load; power and shaft torque from the motor data
Moisture content of the mix	Oven, balance	Drying at 105 [°C] to constant mass
Soil characterisation	Geotechnical laboratory	Particle size distribution, Atterberg limits
Dry density, shrinkage	Balance, calliper	Five bricks, before and after drying
Dry compressive strength	Laboratory press	Three to five specimens after complete drying